

# Near-Optimal Entanglement Distribution in Satellite-Assisted Quantum Networks

Wan-Ting Ho<sup>§||</sup>, Li-Feng Chen<sup>†||</sup>, Jing-Jhih Du<sup>†||</sup>, Jian-Jhih Kuo<sup>†\*</sup>, and Ming-Jer Tsai<sup>§</sup>

<sup>§</sup>Dept. of Computer Science, National Tsing Hua University, Hsinchu, Taiwan

<sup>†</sup>Dept. of Computer Science and Information Engineering, National Chung Cheng University, Chiayi, Taiwan

**Abstract**—Satellite-assisted quantum network (SQN) is emerging as a promising solution to overcome the distance limitations of ground-based fiber quantum network (QN). However, each satellite and ground station has a limited number of transmitters and receivers, respectively, and the Entanglement Distribution Rate (EDR) decreases with the distance between satellites and ground stations, highlighting the need for effective resource allocation to serve requests in the SQN. In this paper, we present a novel optimization problem, termed ESOP, which aims to maximize the total EDR in the network while simultaneously considering the resource capacities of both satellites and ground stations, as well as the fidelity requirements of individual requests. To solve ESOP, we propose a  $(2 + \epsilon)$ -approximation algorithm, AESOP, which combines a greedy approach with a tailored local search. Simulation results show that AESOP achieves up to 64% improvement in total EDR compared to the existing method.

## I. INTRODUCTION

With the rapid advancement of quantum technology, quantum network (QN) significant advantages over classical computing in domains such as quantum teleportation [1], quantum key distribution (QKD) [1], and distributed quantum computing [2]. These applications fundamentally rely on quantum entanglement [3], a phenomenon in which particles become intrinsically correlated, such that the state of one instantaneously influences the other, regardless of distance. Thus, for quantum networks to scale globally, efficient entanglement distribution is needed to reliably share states between distant parties.

One conventional approach to entanglement distribution is through ground-based fiber networks, where entangled photonic qubits are transmitted via optical fiber links between users. However, fiber-based transmission suffers from exponential fidelity (i.e., the quality of entanglement) decay with distance [1]. Due to fiber absorption and scattering losses, the number of entanglements that can be transmitted between users (i.e., the Entanglement Distribution Rate (EDR)) also decreases significantly as the optical fiber distance between users increases, thereby limiting direct fiber-based entanglement to a few hundred kilometers [4]. To mitigate this fiber loss, quantum repeater chains have been proposed to extend entanglement over longer distances [5]. However, practical deployment remains challenging due to stringent requirements on quantum memory coherence time and repeater station infrastructure [6]. Moreover, maintaining large-scale repeater

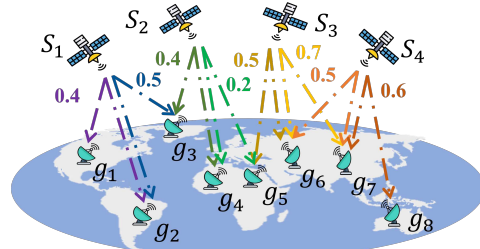


Fig. 1. Example of a Satellite-Assisted Quantum Network.

becomes highly challenging as distance increases [6], making global entanglement distribution over fiber networks difficult.

To overcome these limitations, satellite-assisted quantum network (SQN) has emerged as a promising alternative. Unlike fiber-based links, where fidelity and EDR decrease exponentially with distance, satellite-assisted quantum communication benefits from the near-vacuum environment of space, significantly reducing signal attenuation and allowing entangled photons to propagate over longer distances while preserving high fidelity. This advantage has been validated by successful experimental demonstrations [7]–[9], paving the way for global-scale quantum networks. In SQN [10], satellites are equipped with photon sources that generate entangled photon pairs to facilitate entanglement distribution between two ground stations. Following the double downlink distribution model proposed in [11]–[13], each satellite emits entangled photons via a limited number of transmitters, with each transmitter serving a single ground station pair. Similarly, each ground station is equipped with a limited number of photon receivers, each capable of handling photons from a single satellite. As demonstrated in [7], [9], satellite-based entanglement distribution achieves higher EDR compared to purely fiber-based approaches.

Fig. 1 depicts an example, where  $s_1 - s_4$  represent satellites, and  $g_1 - g_8$  denote ground stations. The weight on each directional arrow from a satellite to a ground station pair indicates the EDR, assuming the satellite emits entangled photon pairs to serve that pair. For instance, satellite  $s_1$  has purple arrows to ground stations  $g_1$  and  $g_2$ , meaning  $s_1$  can serve the request between the ground station pair  $(g_1, g_2)$  with EDR 0.4. For clarity, only arrows from satellites to ground station pairs are shown in Fig. 1 when the corresponding fidelity exceeds the requested fidelity threshold. For example, only  $s_1$  and  $s_2$  satisfy the fidelity requirement for the request between  $(g_2, g_3)$ . Other satellites are omitted as they may fail to meet the threshold due to factors such as low elevation angles or

||: equal contributions; \*: corresponding author (lajacky@cs.ccu.edu.tw)

This work was supported in part by the National Science and Technology Council, Taiwan, under Grants 111-2221-E-007-044-MY3, 111-2628-E-194-001-MY3, 113-2221-E-194-040-MY3, 114-2221-E-007-079-, and 114-2628-E-194-002-MY3.

excessive distance. In this example, suppose that each satellite has only one transmitter and can serve at most one request (i.e., one ground station pair), and each ground station can receive photons from at most one satellite. If a greedy approach is used to assign satellites,  $s_3$  will first serve ground station pair  $(g_6, g_7)$ , as it has the highest EDR 0.7. Next,  $s_1$  will serve the pair  $(g_2, g_3)$ , and  $s_2$  will serve pair  $(g_4, g_5)$ , resulting in a total EDR  $0.7 + 0.5 + 0.2 = 1.4$  in the network. However, a better assignment would have  $s_1$  serve the pair  $(g_1, g_2)$ ,  $s_2$  serve  $(g_3, g_4)$ ,  $s_3$  serve  $(g_5, g_6)$ , and  $s_4$  serve  $(g_7, g_8)$ , achieving a total EDR  $0.4 + 0.4 + 0.5 + 0.6 = 1.9$ , thereby effectively improving the total EDR in the network.

Thus, strategic satellite allocation is essential to maximizing the EDR while ensuring that the fidelity requirements of the requests are met. Although several recent studies [11]–[13] have investigated entanglement distribution in SQN, they either make strong assumptions on the system model, such as assuming each satellite has only one transmitter and each ground station has only one receiver, or fail to provide any approximation ratio guarantees. In light of the above considerations, we make the first attempt to formally explore the *satellite allocation for maximizing the total EDR in the SQN*. Simultaneously determining the admitted requests and their serving satellites while considering fidelity constraints raises the following challenges. 1) *Complicated assignment of satellites to requests*: When each satellite determines its assignment for serving requests, each combination of a satellite and a request can either be selected or not, resulting in an exponential growth in possible allocations between satellites and ground station pairs. As a result, exhaustive enumeration becomes computationally infeasible. Thus, it is crucial to design an efficient algorithm capable of solving the highly complex satellite allocation problem within polynomial time. 2) *Heterogeneous resource allocation*: Each satellite's photon source can support a different number of transmitters, and each ground station has a varying number of photon receivers. Once a transmitter or receiver is reserved for a specific request, it becomes unavailable to others. As a result, how to manage these heterogeneous resources to avoid conflicts becomes crucial. Furthermore, the spatial distribution of satellites and ground stations is highly non-uniform. Some areas may have multiple satellites covering overlapping ground stations, while others are sparsely served. Certain ground stations might only be reachable by specific satellites due to geographical constraints, line-of-sight limitations, or fidelity requirements. If such a satellite does not assign to serve this ground station, the receivers there may remain idle, resulting in underutilized or stranded resources. 3) *Greedy selection trap*: Due to physical factors such as the distance between satellites and ground station pairs, the EDR varies across different combinations of satellites and requests. If a satellite greedily selects and serves requests with the highest EDR in sequence, it may prematurely exhaust its limited photon source resources. This short-sighted allocation may block future opportunities to serve other requests that, while individually offering slightly lower EDR, could together contribute to a higher overall EDR when considered from a

network-wide perspective. To address the above challenges, we formulate a new optimization problem, named **Entanglement Distribution and Satellite Allocation Optimization Problem (ESOP)** in Sec. II. Specifically, given an SQN with a set of requests, ESOP aims to serve a subset of requests that maximize the total EDR in the network, while satisfying their fidelity requirements, the transmitter capacity constraints (i.e., number of transmitters on each satellite), and the receiver capacity constraints (i.e., number of receivers on each ground station). Then, to tackle ESOP, we propose a  $(2 + \epsilon)$ -approximation algorithm, termed **Near-Optimal Algorithm for ESOP (AESOP)** in Sec. III, where  $\epsilon$  is a user-defined tuning knob that balances the trade-off between the approximation ratio and the computational complexity of AESOP. That is, a smaller  $\epsilon$  leads AESOP to produce solutions closer to the optimum, at the cost of increased computation time; conversely, a larger  $\epsilon$  yields faster computation but potentially lower solution quality. Specifically, we first apply a greedy strategy to obtain an initial solution. Subsequently, we devise a refined local search method to improve the initial solution obtained by the greedy approach. Due to page limits, comprehensive related works are provided in Appendix A [14]. Finally, simulation results show that AESOP significantly enhances the total EDR by up to 64% compared to existing methods.

## II. SYSTEM MODEL AND PROBLEM FORMULATION

### A. System Model

An SQN is modeled as an undirected graph  $G = (S, V)$ , where  $S$  represents the set of  $|S|$  satellites, and  $V$  denotes the set of  $|V|$  ground stations. A central controller coordinates the network by communicating with all satellites and ground stations to manage entanglement results and maintain global network information [15]. Each satellite  $s \in S$  is equipped with a quantum photon source that can generate a limited number of entangled photons and support only a fixed number of transmitters on it. These transmitters then emit the entangled photons to ground station pairs. On the other hand, each ground station  $g \in V$  is equipped with a limited number of receivers to collect photons transmitted from satellites. Note that each transmitter can emit entangled photons to only one receiver pair, and each receiver can receive entangled photons from only one transmitter. Moreover, for a satellite  $s$  to be able to serve a ground station  $g$ , the elevation angle  $\theta(s, g)$  between the satellite and the ground station must exceed an elevation angle threshold  $\bar{\theta}$ . Therefore, when a request  $i$  wants to transmit between a ground station pair  $v_s(i), v_t(i) \in V$ , the serving satellite  $s$  must have elevation angles  $\theta(s, v_s(i))$  and  $\theta(s, v_t(i))$  greater than  $\bar{\theta}$  for both  $v_s(i)$  and  $v_t(i)$ . Then, the fidelity of the entangled photon pair received by the request pair  $i$  from the satellite  $s$  can be expressed as a formula in Definition 1.

**Definition 1.** The fidelity  $F(s, i)$  of the entangled photon pair received by request  $i$  from satellite  $s$  can be formulated as [10]:

$$F(s, i) = \frac{1}{4} \left( 1 + \frac{4 \cdot F_0(s)}{(1 + \frac{n(i)}{n(s, i)})^2} \right), \quad (1)$$

where  $F_0(s)$  denotes the initial fidelity of the photons generated by satellite  $s$ , and  $n(i)$  represents the total number of photons received by the receiver of ground station pair  $i$ . Note that in addition to the photons emitted by the satellite, the receiver may also detect photons from environmental noise, such as stray light from external sources (e.g., sunlight or artificial lighting) leaking into the optical system. In addition,  $n(s, i)$  denotes the space-to-ground transmittance between satellite  $s$  and ground station pair  $i$ , primarily determined by the elevation angle, the distance between  $s$  and  $i$ , the wavelength determined by the satellite, as well as other atmospheric conditions [16].

For each request aiming to transmit between its designated ground station pair, a suitable satellite must be assigned to serve it and satisfy the fidelity requirement of the request. Overall, efficiently allocating the resources of satellites and ground stations while maximizing the total EDR in the network constitutes an important optimization problem in SQNs.

### B. Problem Formulation

We formulate the problem based on the system model. The ESOP considers an SQN in which each satellite is equipped with a photon source capable of generating entangled photons to support a limited number of transmitters, which emit the photons to ground station pairs. Besides, each ground station is equipped with a limited number of receivers to collect photons transmitted from the satellites. Let  $R$  be the set of requests. Each request  $i \in R$  aims to establish an entangled pair between its designated ground station pair  $(v_s(i), v_t(i))$  via a satellite. If request  $i$  is served by satellite  $s \in S$ , it is associated with an EDR  $d(s, i) \in \mathbb{R}^+$ , which denotes the number of photons that satellite  $s$  can emit for request  $i$ . Note that the EDR depends on the distance between the satellite and ground station pair as well as the communication protocol used. In general, the rate decreases as the distance increases, as shown in Fig. 3 of [10].

The Entanglement Distribution and Satellite Allocation Optimization Problem (ESOP) seeks to allocate satellite and ground station resources to maximize the total EDR in the SQN, subject to the following constraints: 1) For each satellite  $s \in S$ , the number of ground station pairs it can serve must not exceed the number of transmitters that its photon source can support, denoted as  $c(s)$ . 2) For each ground station  $g \in V$ , the number of satellites from which it can receive photons must not exceed the number of receivers it has  $r(g)$ . 3) For each served request  $i$ , the fidelity achieved by the assigned satellite must be no lower than the required fidelity threshold  $\bar{F}(i)$ .

Let the binary decision variable  $x_{s,i}$  indicate whether the satellite  $s$  is assigned to serve request  $i$ . The integer linear programming (ILP) can be formulated as follows:

$$\underset{x_{s,i}}{\text{maximize}} \sum_{s \in S} \sum_{i \in R} d(s, i) \cdot x_{s,i} \quad (2a)$$

$$\text{subject to } \sum_{i \in R} x_{s,i} \leq c(s), \forall s \in S, \quad (2b)$$

$$\sum_{s \in S} \sum_{i \in R: g=v_s(i) \vee g=v_t(i)} x_{s,i} \leq r(g), \forall g \in V, \quad (2c)$$

$$(F(s, i) - \bar{F}(i)) \cdot x_{s,i} \geq 0, \forall s \in S, i \in R, \quad (2d)$$

$$x_{s,i} \in \{0, 1\} \forall s \in S, i \in R. \quad (2e)$$

The objective (2a) maximizes the total EDR of all requests. Constraints (2b) and (2c) ensure that the resource capacities of satellites and ground stations are not exceeded, respectively. Lastly, Constraint (2d) ensures that the assigned satellite meets the fidelity threshold required by the corresponding request.

Note that the ESOP is NP-hard, as the 3-dimensional matching (3DM) problem [17] can be reduced to the ESOP. Due to the page limit, the proof is provided in Appendix B of [14].

**Theorem 1.** The ESOP is NP-hard.

### III. ALGORITHM DESIGN

To address the aforementioned challenges, we design an approximation algorithm named Near-Optimal Algorithm for **ESOP** (AESOP) with an approximation ratio of  $(2 + \epsilon)$ . To this end, AESOP first computes all candidate satellite assignments for each request that satisfy their respective fidelity thresholds. It then derives an initial solution from the candidate assignments using a greedy-based approach to tackle the first challenge. However, as greedy selection may lead to the issues described in the second and third challenges, AESOP further employs a carefully designed local search to refine the initial solution and address these challenges. In addition, to maintain an approximation ratio of  $(2 + \epsilon)$ , AESOP introduces a novel notion during the local search, termed the *Scaling Factor* and denoted as  $k$ , which is computed based on the user-defined tuning knob  $\epsilon$ . This scaling factor is used to define weights for evaluating whether each assignment in the network is worth selecting to update the initial solution or not.

Overall, the AESOP consists of the three phases: 1) Assignment Space Construction (AS Construction), 2) Initial Solution Generation (IS Generation), and 3) Local Search Optimization (LS Optimization). Specifically, AS Construction first assigns indices to the transmitters of each satellite  $s \in S$  and the receivers of each ground station  $g \in V$ . Then, based on the newly indexed satellites and ground stations, AS Construction constructs a candidate assignment set  $M$ . That is, each assignment  $m \in M$  consists of a specific transmitter on satellite  $s \in S$ , and one receiver on each of the ground stations  $v_s(i)$  and  $v_t(i)$  associated with request  $i \in R$ . This indicates that the transmitter on  $s$  is capable of providing entangled photon pairs to serve the corresponding receiver pair on the ground station pair for the request  $i$ . Besides, each assignment  $m \in M$  is associated with a utility weight  $w(m)$ , corresponding to its EDR  $d(s, i)$ . Next, IS Generation generates an initial solution set  $A$  using a greedy strategy. Concretely, IS Generation iteratively selects the assignment  $m$  with the highest utility weight and adds it to  $A$ . If the transmitter or either of the receivers in  $m$  has already been used in a previous assignment, then  $m$  is considered conflicting and is therefore skipped. This process repeats until no further non-conflicting assignments can be added. Finally, LS Optimization computes the scaling factor  $k$ , which is used to rescale the utility weights of all assignments, regardless of whether they are included in  $A$ . It then performs a refined local search based

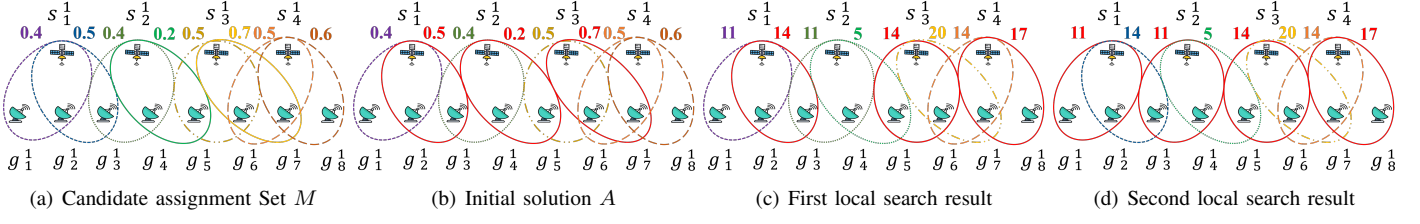


Fig. 2. An example of AESOP.

on the rescaled utility weights. A larger value of  $k$  encourages the local search to explore more assignments by performing more iterations and prioritizing solution quality, at the cost of increased computational time.

**1) AS Construction:** AS Construction first assigns indices to all transmitters on the satellites and receivers on the ground stations to facilitate the construction of the candidate assignment  $M$ . For example, if a satellite  $s$  is equipped with three transmitters, they are indexed as  $s^1, s^2$ , and  $s^3$ . Similarly, if ground station  $g$  has two receivers, they are indexed as  $g^1$  and  $g^2$ . Based on the indexed network, AS Construction iterates over all combinations of transmitters and receiver pairs to form valid candidate assignments  $M$ . For instance, suppose transmitter  $s^1$  is selected to serve request  $i$ , which is associated with receivers  $v_s(i)^1$  and  $v_t(i)^2$ . AS Construction then checks whether the fidelity between satellite  $s$  and the corresponding ground stations  $v_s(i)$  and  $v_t(i)$  satisfies the fidelity threshold  $\bar{F}(i)$ . If the fidelity constraint is met, the corresponding assignment  $m$  is added to  $M$  with its utility weight  $w(m)$  set to the EDR  $d(s, i)$ . Note that at this step, the resource capacities of satellites and ground stations are not considered. Any transmitter-receiver pair combination that meets the fidelity requirement is regarded as a valid assignment. The fidelity is computed according to Eq. (1) and is mainly influenced by the photon's initial fidelity, the elevation angles between the satellite and the ground stations, and the transmission distance between them.

**Example 1.** In Fig. 2(a), based on the example in Fig. 1, we illustrate how AS Construction generates the candidate assignment set  $M$ . As each satellite  $s_1-s_4$  and ground station  $g_1-g_8$  has exactly one transmitter and one receiver, AS Construction first assigns indices to these components. Specifically, the transmitter on satellite  $s_1$  is indexed as  $s_1^1$ , and the receiver on ground station  $g_1$  as  $g_1^1$ , respectively for the others. Next, AS Construction generates the candidate assignment set  $M$ . Since all combinations satisfying the fidelity threshold have been indicated in Fig. 1, circles represent candidate assignments and are labeled from left to right as  $m_1$  to  $m_8$ . For example, the purple dotted circle  $m_1$  denotes an assignment where transmitter  $s_1^1$  serves the receiver pair  $(g_1^1, g_2^1)$ . The number next to each circle indicates its corresponding utility weight, such as  $w(m_1) = d(s_1^1, (g_1^1, g_2^1)) = 0.4$  for the purple one. ■

**2) IS Generation:** To handle the intricate assignment between transmitters and receivers, IS Generation constructs an initial solution set  $A \subseteq M$  through a greedy selection strategy. To build  $A$ , at each iteration, IS Generation selects the assignment with the highest utility weight from  $M$ . If the

selected assignment involves any transmitter or receiver already used by a previously selected assignment, it is considered conflicting and is skipped. This process continues until no further non-conflicting assignments can be added to  $A$ .

**Example 2.** Fig. 2(b) further illustrates how IS Generation constructs the initial solution set  $A$ , represented by red circles. IS Generation first selects the yellow dotted circle  $m_6$  with the highest utility weight  $w(m_6) = 0.7$ , and adds it to  $A$ . Next, the brown dotted circle  $m_8$  is skipped due to a conflict with  $m_6$ . Then, the blue dotted circle  $m_2$  is added to  $A$ . Subsequently,  $m_5$  and  $m_7$  are skipped for conflicts with  $m_6$ . Following this greedy strategy, IS Generation continues until no further non-conflicting assignments can be added. The final selected initial solution set  $A$  is highlighted in red circles. ■

**3) LS Optimization:** Before introducing how the refined local search improves the solution, we first compute the scaling factor  $k$  and then present two key structures used in the local search process. The scaling factor  $k$  is determined by the user-defined tuning knob  $\epsilon > 0$ , where a smaller  $\epsilon$  indicates a stronger preference for an approximation ratio closer to the optimum. Consequently, a larger  $k$  is computed, encouraging the local search to perform more iterations and prioritize solution quality. The scaling factor  $k$  is calculated by:

$$k = \lceil \frac{2}{\epsilon} \rceil + 1. \quad (3)$$

Once  $k$  is determined, IS Generation updates the utility weight of each assignment  $m \in M$ , regardless of whether it is selected into the set  $A$ . Let  $w(A)$  denote the sum of utility weights of all assignments in  $A$ . The updated weight is computed as:

$$w(m) \leftarrow \lfloor w(m) \cdot \frac{k \cdot |M|}{w(A)} \rfloor. \quad (4)$$

Next, we describe the underlying structures used in the local search: *branches* and their corresponding *offshoots*. In brief, the refined local search explores a branch that is not fully included in the current solution set  $A$ . If the offshoots stemming from such a branch can improve the current solution, the conflicting assignments are replaced with this offshoot cluster. Specifically, a branch  $B$  consists of a center assignment  $n_B(m)$  and a cluster of offshoots  $C_B$ , where each offshoot  $o_B(m) \in C_B$  is also an assignment. Each offshoot shares at least one transmitter or receiver with the center, and all offshoots in the same cluster are pairwise disjoint, meaning no two offshoots share a transmitter or receiver. Based on these structures, the refined local search iteratively updates the initial solution set  $A$  obtained from IS Generation. In each iteration,

LS Optimization searches for a branch  $B$  not fully contained in  $A$ . Let  $C_B$  denote the offshoot cluster and  $L$  represent the set of conflicting assignments between  $A$  and  $C_B$ . If the squared utility weight satisfies  $w^2(C_B) > w^2(L)$ , LS Optimization updates the solution set by replacing  $L$  with  $C_B$ :

$$A \leftarrow (A \setminus L) \cup B. \quad (5)$$

This refined local search repeats until no further improving branch can be found.

**Example 3.** Fig. 2(c) and Fig. 2(d) illustrate the first and second iterations of the refined local search in LS Optimization, respectively. In Fig. 2(c), LS Optimization first updates all the utility weight according to Eq. (4). Given  $\epsilon = 0.5$ , the scaling factor is  $k = \lceil \frac{2}{0.5} \rceil + 1 = 5$ . With  $|M| = 8$ , and  $w(A) = 0.5 + 0.2 + 0.7 = 1.4$ , the updated utility weight of  $m_1$  is  $\lfloor w(m_1) \cdot \frac{k \cdot |M|}{w(A)} \rfloor = \lfloor 0.4 \cdot \frac{5 \cdot 8}{1.4} \rfloor = 11$ . Following the same procedure, all other utility weight are similarly updated.

Then, LS Optimization identifies a branch  $B$  centered at  $m_6$  with two offshoots  $m_5$  and  $m_8$ . Based on the current solution set  $A = \{m_2, m_4, m_6\}$ , the conflicting assignment set for such  $B$  is  $L = \{m_4, m_6\}$ , since  $m_4$  conflicts with  $m_5$ , and  $m_6$  conflicts with both  $m_5$  and  $m_8$ . As  $w^2(C_B) = 14^2 + 17^2 = 485$  exceeds  $w^2(L) = 5^2 + 20^2 = 425$ , LS Optimization updates the solution set  $A$  as shown by the red circles in Fig. 2(c). Subsequently, in Fig. 2(d), LS Optimization finds another branch  $B$  centered at  $m_2$  with two offshoots  $m_1$  and  $m_3$ . Based on the updated solution set, the conflicting assignment set is  $L = \{m_2\}$ . Since  $w^2(C_B) = 11^2 + 11^2 = 242$  exceeds  $w^2(L) = 14^2 = 196$ , the solution set  $A$  is updated again, as shown in Fig. 2(d). At this point, no further improving branch can be found, and the refined local search terminates. ■

The AESOP is a  $(2 + \epsilon)$ -approximation algorithm. Due to the page limit, the proof is presented in Appendix C of [14].

**Theorem 2.** The AESOP is a  $(2 + \epsilon)$ -approximation algorithm for the ESOP, where  $\epsilon$  is a user-defined parameter.

#### IV. PERFORMANCE EVALUATION

##### A. Simulation Settings

Extensive simulations are conducted to compare AESOP with three baseline methods: OPT-SAT [11], BACKOFF [13] and GREEDY. Note that, BACKOFF refers to the GREEDY\_BACKOFF method proposed in [13], and GREEDY corresponding to AESOP without LS Optimization. In each simulation, one parameter is varied while all others are fixed at their default values. To generate the network, following the setup in [15], 137 ground stations are randomly deployed across 6 Europe countries with one ground station per city. Satellite configurations are generated using the orbit simulator in [18], recording the positions of 100 Low Earth Orbit satellites, ensuring that each satellite can serve at least one request for feasibility. Each satellite is randomly assigned 1 to 4 transmitters, and each ground station 2 to 6 receivers. We set the fidelity threshold  $F(i) = 0.8$  for each request, with  $F_0(s) = 1$  and  $\bar{\theta} = 20^\circ$  [12]. For calculating the number

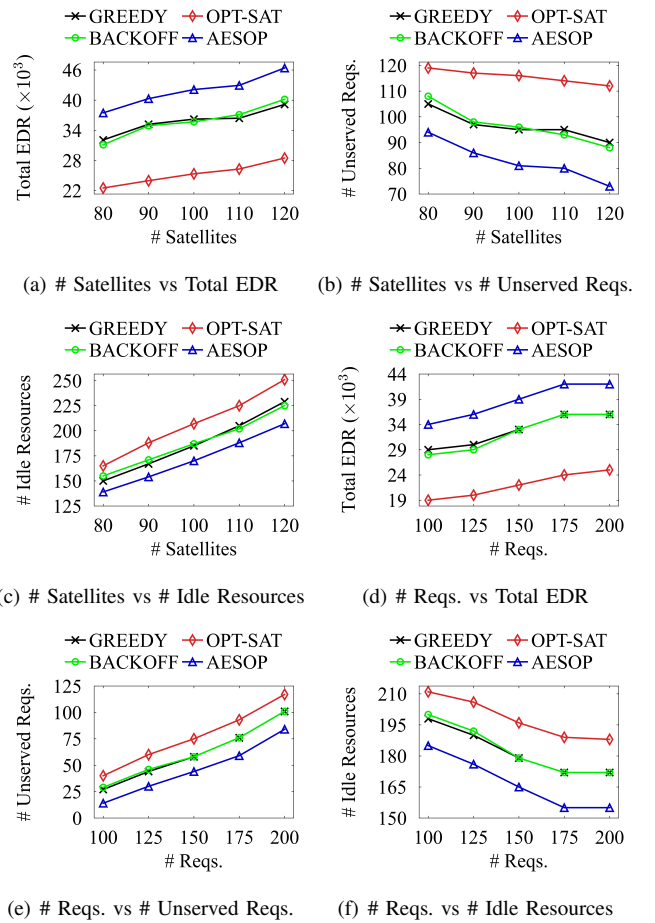


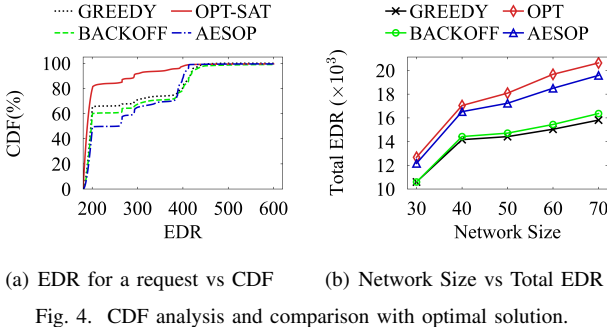
Fig. 3. Effect of the number of satellites and requests on different metrics.

of photons received by the receiver  $n(i)$ , and the space-to-ground transmittance  $n(s, i)$ , we adopt the loss and noise model [10]–[12], where the atmospheric extinction coefficient is set to 0.028125, and the wavelength to 735 nm. The default number of requests is 200. The EDR between each satellite and ground station pair is determined based on simulation results from [10], primarily depending on their distance. We evaluate all methods by the following metrics: 1) *Total EDR*: the total EDR achieved in the network. 2) *# Unserved Requests*: the number of requests remaining unserved after allocation. 3) *# Idle Resources*: the number of transmitters remaining unused after allocation. 4) *CDF*: the cumulative percentage of requests with the EDR less than or equal to a specified value. In the figures, requests are abbreviated as *Reqs.*, and each result is averaged over 30 trials. More experiment results are provided in Appendix D of [14] due to page limits.

##### B. Numerical Results

Overall, the AESOP outperforms all other approaches, as shown in Figs 3 and 4, by effectively allocating resources to serve requests and addressing all the challenges.

1) *Effect of Number of Satellites*: Figs. 3(a)–3(c) illustrate the impact of the number of satellites on different metrics. In Fig. 3(a), as the number of satellites increases, the total EDR improves across all methods. AESOP consistently



(a) EDR for a request vs CDF      (b) Network Size vs Total EDR

Fig. 4. CDF analysis and comparison with optimal solution.

achieves the highest total EDR, benefiting from the use of local search in LS Optimization, which refines the solution by exploring branches within the candidate assignment set. This highlights AESOP's strong capability in addressing the third challenge. Furthermore, Fig. 3(b) shows that increasing the number of satellites also increases the number of served requests, leading to a reduction in unserved requests. AESOP consistently maintains the lowest number of unserved requests among all methods. In conjunction with Fig. 3(c), AESOP not only serves more requests, but also utilizes a greater portion of available transmitters, resulting in fewer idle resources. This confirms that greedy selection combined with local search enables AESOP to explore more effective satellite resource allocation strategies, thereby addressing the second challenge. Compared to OPT-SAT, BACKOFF, and GREEDY, AESOP improves total EDR by up to 64%, 16%, and 19%, respectively.

*2) Effect of Number of Requests:* Figs. 3(d)–3(f) show the effect of request numbers on different metrics. In Figs. 3(d) and 3(e), AESOP achieves higher total EDR and serves more requests than all baselines. As requests increase, while satellites and ground stations remain fixed, the available resources in the network stay constant, limited resources intensify competition. Consequently, serving a request that consumes critical resources may block overlapping requests that would otherwise contribute to a higher overall EDR, thus exacerbating local minimum issues. Therefore, the allocation rule becomes even more critical. In AESOP, LS Optimization evaluates the quality of each assignment using squared utility weight. This mechanism enables AESOP to achieve higher total EDR and serve more requests, outperforming all other baseline methods. Fig. 3(f) further shows that as the number of requests grows, AESOP consistently utilizes satellite resources more effectively than other methods, once again demonstrating its strong capability in addressing the second challenge.

*3) CDF Analysis and Comparison with the Optimal Solution:* Fig. 4(a) shows the *CDF* of requests with allocated EDR at or below a given value. Compared to other methods that often yield low EDR for many requests, AESOP more effectively allocates satellite resources, enabling most requests to achieve high EDR. This highlights the strength of combining greedy with local search in addressing both satellite allocation and request admission. Fig. 4(b) compares AESOP with the optimal solution in a small-scale network. OPT denotes the optimal solution computed by the Gurobi solver. OPT-SAT is omitted as its results significantly deviate from the optimal.

Network size indicates the number of satellites and ground stations (e.g., size 30 means 30 of each). To maintain computational feasibility, each satellite and ground station is adjusted to equip with 1 to 3 transmitters and receivers. The small scale is necessary because solving the optimal case for sizes beyond 80 needs several hours. As shown, AESOP achieves near-optimal performance in polynomial time with slight degradation.

## V. CONCLUSIONS

In this paper, we first examine the limitations of ground-based fiber QN and explore an SQN based on double down-link distribution. Although this architecture mitigates distance-induced fidelity and EDR degradation, it introduces new challenges in satellite allocation, due to the scarcity and heterogeneity of resources across satellites and ground stations. To address these challenges, we formulate an optimization problem, ESOP, which aims to maximize the total EDR while satisfying fidelity and resource constraints. We then propose ESOP, a  $(2 + \epsilon)$ -approximation algorithm, AESOP that combines a greedy selection strategy with a novel local search approach. Besides, the user-defined tuning parameter  $\epsilon$  allows balancing the trade-off between approximation ratio and computation efficiency. Finally, simulation results demonstrate that AESOP outperforms other methods up to 64%.

## REFERENCES

- [1] H.-J. Briegel *et al.*, “Quantum repeaters: the role of imperfect local operations in quantum communication,” *Phys. Rev. Lett.*, vol. 81, pp. 5932 – 5935, 1998.
- [2] M. Caleffi *et al.*, “Distributed quantum computing: a survey,” *Comput. Netw.*, vol. 254, p. 110672, 2024.
- [3] R. Horodecki *et al.*, “Quantum entanglement,” *Rev. Mod. Phys.*, vol. 81, pp. 865–942, 2009.
- [4] S. P. Neumann *et al.*, “Continuous entanglement distribution over a transnational 248 km fiber link,” *Nat. Commun.*, vol. 13, p. 6134, 2022.
- [5] J. Li *et al.*, “Fidelity-guaranteed entanglement routing in quantum networks,” *IEEE Trans. Commun.*, vol. 70, pp. 6748–6763, 2022.
- [6] K. Azuma *et al.*, “Quantum repeaters: From quantum networks to the quantum internet,” *Rev. Mod. Phys.*, vol. 95, p. 045006, 2023.
- [7] S.-K. Liao *et al.*, “Satellite-to-ground quantum key distribution,” *Nature*, vol. 549, pp. 43–47, 2017.
- [8] J.-G. Ren *et al.*, “Ground-to-satellite quantum teleportation,” *Nature*, vol. 549, pp. 70–73, 2017.
- [9] Y.-A. Chen *et al.*, “An integrated space-to-ground quantum communication network over 4,600 kilometres,” *Nature*, vol. 589, pp. 214–219, 2021.
- [10] S. Khatri *et al.*, “Spooky action at a global distance: analysis of space-based entanglement distribution for the quantum internet,” *npj Quantum Inf.*, vol. 7, p. 4, 2021.
- [11] N. K. Panigrahy *et al.*, “Optimal entanglement distribution using satellite based quantum networks,” in *IEEE INFOCOM WKSHPS*, 2022.
- [12] X. Wei *et al.*, “Optimal entanglement distribution problem in satellite-based quantum networks,” *IEEE Netw.*, vol. 39, pp. 97–103, 2025.
- [13] A. Williams *et al.*, “Scalable scheduling policies for quantum satellite networks,” in *IEEE QCE*, 2024.
- [14] W.-T. Ho *et al.*, “Near-optimal entanglement distribution in satellite-assisted quantum networks (appendix),” Aug 2025. [Online]. Available: <https://github.com/Sunny-Ho/25-GC-Satellite>
- [15] S.-M. Huang *et al.*, “Socially-aware concurrent entanglement routing in satellite-assisted multi-domain quantum networks,” in *IEEE ICC*, 2023.
- [16] L. Jintao *et al.*, “Link budget analysis for free-space optical satellite networks,” in *IEEE WoWMoM*, 2022.
- [17] D. P. Williamson and D. B. Shmoys, *The Design of Approximation Algorithms*. Cambridge Univ. Press, 2011.
- [18] F. R. Hoots and R. L. Roehrich, “Spacetrack report no. 3: Models for propagation of NORAD element sets,” Aerospace Def. Center, Peterson AFB, Tech. Rep., 1980.